Synthesis, Characterization, and Electrocatalytic Activity of PtBi and PtPb Nanoparticles Prepared by Borohydride Reduction in Methanol

Chandrani Roychowdhury,[†] Futoshi Matsumoto,[†] Varvara B. Zeldovich,[†] Scott C. Warren,[‡] Paul F. Mutolo,[†] MariaJulieth Ballesteros,[†,§] Ulrich Wiesner,[‡] Héctor D. Abruña,*[,†] and Francis J. DiSalvo*[,†]

Department of Chemistry and Chemical Biology, Baker Laboratory, and Department of Materials Science and Engineering, Cornell University, Ithaca, New York 14853

Received February 27, 2006. Revised Manuscript Received May 4, 2006

Intermetallic compounds PtPb and PtBi have been prepared in nanoparticle form by dissolving Pt and Pb or Bi precursors in anhydrous methanol and coreducing the metal precursors with sodium borohydride. The average domain size determined from pXRD is 10 nm. The particles have been characterized by pXRD, SEM, STEM, EDX, and CBED. SEM and STEM images show the particles to be aggregated, forming clusters and chains. The BET surface area of the nanoparticles was measured using Kr as the adsorbing gas. The electrocatalytic oxidation of formic acid and methanol by the as-prepared PtPb and PtBi nanoparticles has been studied by rotating disk voltammetry for potential fuel-cell applications. The PtPb and PtBi nanoparticles displayed enhanced electrochemical activity toward formic acid and methanol oxidation when compared to commercially available Pt and PtRu nanoparticles. The electrocatalytic activity of the PtPb nanoparticles was studied as a function of sonication time of the catalyst ink, and morphology changes were followed by scanning electron microscopy. The results showed that the activity of the catalyst initially increased with sonication time and then decreased.

Introduction

In the past decade, interest in the direct conversion of chemical energy to electricity via fuel cells has received increasing attention. The use of fuel cells can circumvent Carnot cycle limitations and can, in principle, supply energy with efficiencies in excess of 80%, depending on the fuel used.[1] Fuel cells are indeed attractive alternatives to combustion engines in transportation applications for electrical power generation because of their high efficiencies and low pollution-generation levels. Among fuel-cell technologies, polymer electrolyte membrane (PEM) fuel cells are generally considered to be the most viable approach for mobile applications.[2] In addition, there has also been increasing interest in developing direct methanol fuel cells (DMFC) as a power source for small portable electronic devices.[3,4]

Of the common fuels generally considered, hydrogen is mechanistically the easiest to oxidize and produces no CO_2, so it is often seen as a likely fuel for fuel cells. In fact, this is one of the central tenets of the so-called hydrogen economy. However, H_2/O_2 fuel cells require either on-site H_2 storage or an on-board reformer to extract H_2 from organic fuels. Steam reformation is a high-temperature (∼650 °C, depending on the fuel[1]) technique in which the fuel is combined with water to form carbon dioxide, carbon monoxide, and hydrogen. However, this mixture of gases needs to be purified before its introduction into a fuel cell, because the CO interacts strongly with current catalysts, drastically reducing their activity (catalyst poisoning) and performance. As an alternative, and for smaller, portable applications, there has been a growing drive to study the direct electrocatalytic oxidation of small organic molecules (SOMs) for potential use as fuels in so-called direct fuel cells.[5] For oxidizing any fuel, it is imperative to have an electrocatalyst that can support high rates of fuel use or, equivalently, the current densities that are needed for practical applications. Platinum-based catalysts are some of the most-efficient catalyst materials available for oxidation of SOMs.[6] Indeed, Pt is an excellent catalyst for the dehydrogenation of fuels, but as mentioned earlier, it is easily poisoned by the CO that results from partial oxidation of the SOM. Indeed, catalysts that are useful for SOM oxidation should also be efficient catalysts for quite impure hydrogen. Oxidation of most candidate fuels also requires the catalytic surface to be a source of oxygen for facilitating the oxidation of CO (and other intermediates) to carbon dioxide. Pt is also highly vulnerable to other

* To whom correspondence should be addressed. E-mail: hda1@cornell.edu (H.D.A.), fjd3@cornell.edu (F.J.D.).

[†] Department of Chemistry and Chemical Biology, Baker Laboratory, Cornell University.

[‡] Department of Materials Science and Engineering, Cornell University.

[§] Present address: Department of Chemistry, The City College of New York.

(1) Lamy, C. L.; Leger, J.-M.; Srinivasan, S. *Direct Methanol Fuel Cells: From a Twentieth Century Electrochemist's Dream to a Twenty-First Century Emerging Technology*; Kluwer Academic/Plenum Publishers: New York, 2001; Vol. 34.

(2) Haile, S. M.; Boysen, D. A.; Chisholm, C. R. I.; Merle, R. B. *Nature* **2001**, *410*, 910.

(3) Reddington, E.; Sapienza, A.; Gurau, B.; Viswanathan, R.; Sarangapani, S.; Somtkin, E. S.; Mallouk, T. E. *Science* **1998**, *280*, 1735.

(4) Ross, P. N. *Electrocatalysis*; Lipkowski, J., Ross, P. N., Eds.; Wiley-VCH: New York, 1998; Chapter 2.

(5) Parsons, R.; VanderNoot, T. *J. Electroanal. Chem.* **1988**, *257*, 9.

(6) Schmidt, T. J.; Gasteiger, H. A.; Behm, R. J. *J. Electrochem. Soc.* **1999**, *146*, 1296.

10.1021/cm060480e CCC: $33.50
Published on Web 06/13/2006

poisons, such as sulfur (often in the form of thiols or thiophenes), halides, and other species. These poisons remain strongly adsorbed on the platinum surface, thus greatly reducing efficiency and overall performance of fuel cells.

To minimize poisoning, researchers have used Pt-based alloys, especially PtRu, as bifunctional catalysts, in which the platinum activates the fuel to dehydrogenation and the other metal(s) are thought to provide the necessary oxygen for complete oxidation of the fuel to CO_2. Indeed, PtRu alloys have shown relative tolerance to CO poisoning, increased current densities, and a decreased overpotential for fuel oxidation[6−8] when compared to pure platinum. In fact, PtRu remains the industry and research standard, and in recent years, the primary direction of fuel cell anode development for SOM fuels has been in the enhancement of PtRu-based systems. As such, the materials employed as anodes have remained virtually unchanged for decades but have been better-engineered to improve performance.[1−7] Such efforts include important advances in making 3−5 nm diameter particles of the electrocatalysts,[9,10] refining the composition of the catalyst,[11−13] and surface structure elucidation of the purported active form of the catalysts.[7,14,15] However, even PtRu still suffers from a significant overpotential for the oxidation of organic fuels and from poisoning by sulfur-containing compounds, each of which result in severe loss of catalytic efficiency. Furthermore, as with all alloys (better described as solid solutions), PtRu has a poorly defined surface structure, with its surface sites occupied by Pt or Ru in a random fashion. In addition, the use of Ru-based alloys in place of pure Pt introduces a stability problem: during extended periods of operation, particularly under nonoptimal usage (especially at high temperatures and current densities), the alloy surface becomes depleted of Ru.[16,17] Ru has a higher surface energy than Pt, and eventually will migrate into the bulk. Ru has also been reported to dissolve and nucleate in other parts of the cell if the anode potential becomes too positive, which in turn can facilitate degradation of the cathode as well as the membrane[16] that separates the anode and the cathode. This breakdown of the membrane causes decreased proton conduction to the cathode as well as fuel cross over, which further diminish efficiency.

We recently reported[18,19] on a new approach in the search for electrocatalysts to replace PtRu with less-expensive materials and avoid problems inherent in using disordered alloys as catalysts, such as segregation and poisoning by CO and sulfur-containing materials, as mentioned earlier. In place of the disordered PtRu alloy, ordered intermetallic phases, such as PtBi and PtPb, were shown to be excellent electrocatalysts for formic acid oxidation. As bulk materials, both PtBi and PtPb exhibit high electrocatalytic activity toward formic acid oxidation and essentially complete tolerance toward poisoning by CO.[18,19] However, for these materials to be incorporated into fuel cells, they need to be prepared in nanoparticle form, so as to have increased surface area to support the required current densities.

Nanophase powders of elemental metals and some of their alloys are currently used in a variety of technical fields because they possess specific and remarkable properties. Because of their high proportion of surface vs bulk atoms, the reactivity per unit mass of these materials is significantly higher than that of coarse particles, making them ideal candidates for powder metallurgy or for catalytic applications. Metal nanoparticles for catalytic applications have been prepared by various techniques, but most often by chemical reduction and precipitation from aqueous or organic solutions.[20−26] Reduction by sodium borohydride is a common and popular method for synthesis of metal nanoparticles.[27−29] Sodium borohydride has especially been used as a reducing agent to prepare nanoparticles of bimetallic alloys such as Pt− Ni[30] and Pt−Ru[31] for use as electrocatalysts for methanol oxidation. However, most reactions used to prepare nanoparticles of alloys with $NaBH_4$ as reducing agent use water as the solvent. Sodium borohydride is stable in water only at pH > 10. In acidic or neutral aqueous solutions, it reacts quite vigorously, liberating hydrogen gas. This makes it difficult to control the stoichiometry of the reactions, because much of the reducing agent gets used up in reducing the solvent. On the other hand, sodium borohydride is kinetically much more stable in alcohols, such as methanol, ethanol, etc.[32] These solvents are attractive for the synthesis of metallic and bimetallic nanoparticles by reduction using sodium borohydride. Although sodium borohydride has been

(7) Costamanga, P.; Srinivisan, S. *J. Power Sources* **2001**, *102*, 242.
(8) Narayanan, S. R.; Chun, W.; Valdez, T. I.; Jeffries-Nakamura, B.; Frank, H.; Surampudi, S.; Halpert, G.; Kosek, J.; Cropley, C.; LaConti, A. B.; Smart, M.; Wang, Q. J.; Prakash, G. S.; Olah, G. *Fuel Cell Seminar Abstract Book*; Fuel Cell Seminar, Orlando, FL, Nov 17−20, 1996; p 525.
(9) Gasteiger, H. A.; Markovic, N. M.; Ross, P. N. *J. Phys. Chem.* **1995**, *99*, 8290.
(10) Long, J. W.; Stroud, R. M.; Swider-Lyons, K. E.; Rolison, D. R. *J. Phys. Chem. B* **2000**, *104*, 9772.
(11) Lee, C. E.; Tiege, P. B.; Zing, Y.; Nagendran, J.; Bergens, S. H. *J. Am. Chem. Soc.* **1997**, *119*, 3543.
(12) Lee, C. E.; Bergens, S. H. *J. Electrochem. Soc.* **1998**, *145*, 4182.
(13) Mallouk, T. E.; Smotkin, E. S.; Reddington, E.; Sapienza, A.; Lafrenz, T. J.; Chan, B. C.; Gurau, B.; Viswanathan, R.; Liu, R.; Sarangapani, S.; Ley, K. L. *J. Phys. Chem. B* **1998**, *102*, 9997.
(14) Chrzanowski, W.; Wieckowski, A. *Langmuir* **1998**, *14*, 1967.
(15) Chrzanowski, W.; Wieckowski, A. *Langmuir* **1997**, *13*, 5974.
(16) Dr. Grant Ehrlich, UTC Fuel Cells, private communication, 2006.
(17) Dr. Shimshon Gottesfeld, MTI Micro Fuel Cells, private communication, 2006.
(18) Casado- Rivera, E.; Volpe, D. J.; Alden, L.; Lind, C.; Downie, C.; Vázquez- Alvarez, T.; Angelo, A. C. D.; DiSalvo, F. J.; Abruña, H. D. *J. Am. Chem. Soc.* **2004**, *126*, 4043.
(19) Casado Rivera, E.; Gal, Z.; Angelo, A. C. D.; Lind, C.; DiSalvo, F. J.; Abruña, H. D. *Chem. Phys. Chem.* **2003**, *4*, 193.
(20) Komarneni, S.; Li, D.; Newalkar, B.; Katsuki, H.; Bhalla, A. S. *Langmuir* **2002**, *18*, 5959.
(21) Alivisatos, A. P. *Science* **1996**, *271*, 933.
(22) Ahmadi, T. S.; Wang, Z. L.; Green, T. C.; Henglein, A.; El-Sayed, M. A. *Science* **1996**, *272*, 1924.
(23) Pileni, M. P. *Langmuir* **2001**, *17*, 7476.
(24) Teranishi, T.; Hosoe, M.; Tanaka, T.; Miyake, M. *J. Phys. Chem. B* **1999**, *103*, 1805.
(25) Cushing, B. L.; Kolesnichenko, V. L.; O'Connor, C. J. *Chem. Rev.* **2004**, *104*, 3893.
(26) Devairaj, T. C.; Chen, W.; Lee, J. Y. *J. Mater. Chem.* **2003**, *13*, 2555.
(27) Scott, R. W. J.; Sivadinarayana, C.; Wilson, O. M.; Yan, Z.; Goodman, W.; Crooks, R. J. *J. Am. Chem. Soc.* **2005**, *127*, 1380.
(28) Maye, M. M.; Lim, I. S.; Luo, J.; Rab, Z.; Rabinovich, D.; Liu, T.; Zhong, C.-J. *J. Am. Chem. Soc.* **2005**, *127*, 1519.
(29) Roucoux, A.; Schulz, J.; Patin, H. *Chem. Rev.* **2002**, *102*, 3762.
(30) Antolini, E.; Salgado, J. R. C.; dos Santos, A. M.; Gonzalez, E. R. *Electrochem. Solid-State Lett.* **2005**, *8*, A226.
(31) Chai, G. S.; Yoon, S. B.; Yu, J.; Choi, J.; Sung, Y. *J. Phys. Chem. B* **2004**, *108*, 7074.
(32) Fieser, L. F.; Fieser, M. *Reagents for Organic Synthesis*; John Wiley: New York, 1967; Vol. 1, p 1050.

used as a reducing agent to make nanoparticles of alloys, there has been very little published work on its use in preparing nanoparticles of ordered intermetallic compounds. Schaak et al.[33] have used sodium borohydride coupled with a polyol solvent to make nanocrystals of the ternary intermetallic compounds $AuCuSn_2$ and $AuNiSn_2$. However, it is clear that the ternary phase develops only at higher temperatures through solid-state reaction of inhomogeneous particles.

In this paper, we present the synthesis, characterization, and electrochemical activity of nanoparticles of the ordered intermetallic compounds PtBi and PtPb using anhydrous methanol as the solvent and sodium borohydride as the reducing agent. Chlorides of platinum and lead and bismuth salts of (2-[2-{2-methoxy}ethoxy]ethoxy)acetic acid (MOEEAA) were used as the precursors. Characterization of the products was performed using powder X-ray diffraction (pXRD), scanning electron microscopy (SEM), scanning transmission electron microscopy (STEM), convergent beam electron diffraction (CBED), electron energy-loss spectroscopy (EELS), and energy-dispersive X-ray microanalysis (EDX). The surface area of the nanoparticles has also been measured via BET using krypton as the adsorbing gas. The electrocatalytic activity of both of the intermetallic phases toward oxidation of formic acid and methanol has been studied by rotating disk voltammetry. As mentioned elsewhere,[18] oxidation of formic acid is useful as a model system for studying the electrochemical oxidation of simple alcohols (e.g., methanol, ethanol) and, on Pt, CO is produced as a poisoning intermediate. The as-prepared PtBi and PtPb nanoparticles exhibited enhanced electrocatalytic activity when compared to that of commercially available Pt and PtRu, in terms of both onset potential for oxidation and surface area normalized current density. The PtPb nanoparticles also exhibited high surface area normalized current density for methanol oxidation. The electrocatalytic activity of the PtPb nanoparticles has also been studied as a function of sonication time of the catalyst ink and has been followed by scanning electron microscopy. The results show that the activity of the catalyst initially increases with sonication time but then decreases.

Experimental Section

Materials. With the exception of Bi and Pb MOEEAA compounds, all materials used were reagent grade. $H_2PtCl_6 \cdot 6H_2O$ (Strem Chemicals) was used as the platinum precursor. $Bi(MOEEAA)_3$ was prepared by reacting stoichiometric amounts of bismuth acetate (99.999%, Alfa Aesar) and (2-[2-{2-methoxy}ethoxy]ethoxy)acetic acid (MOEEAA) (Aldrich). Acetic acid was formed as a side product and removed by rotatory evaporation. The final product, $Bi(MOEEAA)_3$, was collected as a colorless, viscous liquid and stored in an argon-filled glovebox. $Pb(MOEEAA)_2$ was prepared in the same way, using lead acetate (Aldrich) as the starting material. Anhydrous methanol (Alfa Aesar) was used as solvent. $NaBH_4$ (Aldrich) was used as the reducing agent. Degassed distilled water and acetone (Aldrich) were used to wash the final products. The water was purified with a Millipore Milli Q system.

Synthesis of Nanoparticles. All reactions were done using standard Schlenk line techniques, under an inert gas (argon) atmosphere. Anhydrous methanol (50 mL) was degassed with argon for 2 h. To synthesize PtPb nanoparticles, we dissolved between 0.15 and 0.25 g of $Pb(MOEEAA)_2$ in the degassed methanol. A stoichiometric amount, relative to the lead precursor, of the $H_2PtCl_6 \cdot 6H_2O$ was dissolved in 10 mL of degassed anhydrous methanol and added to the lead precursor solution. Between 0.2 and 0.3 g of $NaBH_4$ (10−20-fold excess equivalents, on the basis of the assumption that each $NaBH_4$ molecule donates one electron) was weighed into a test tube, to which 15 mL of degassed anhydrous methanol was added. This solution was immediately added to the metal precursor solution. There was instant bubbling, and a black particulate product formed, which precipitated out of the solution within 10 min. The clear solution and the black product were stirred under argon for 12 h. The solid product was then separated from the supernatant liquid by decantation and centrifugation; it was subsequently washed three times each with distilled water and acetone in order to remove the side products and other organic phases that may have formed during the reaction. After each washing step, the solids were also separated from the liquid by centrifugation. Afterward, the powders were dried under vacuum at room temperature.

PtBi nanoparticles were prepared in the same way as discussed above, with the exception of using $Bi(MOEEAA)_3$ as the starting precursor instead of $Pb(MOEEAA)_2$.

Characterization. An X-ray powder diffraction powder pattern (Scintag XDS 2000) was taken of the black PtBi and PtPb nanoparticles to confirm the composition and structure of the intermetallic phase. The particle morphology and size were studied by scanning electron microscopy (SEM) using a LEO-1550 Field Emission SEM (FE-SEM). Scanning TEM images, energy-dispersive analysis by X-rays (EDX), electron energy-loss spectroscopy data (EELS), selected area electron diffraction (SAED), and convergent beam electron diffraction (CBED) data were collected on a VG HB501UX UHV-STEM. Suspensions of nanoparticles were used to obtain SEM and STEM data. To prepare the suspensions, we added 2−5 mg of nanoparticles to 10 mL of degassed isopropyl alcohol. The solutions were sonicated using a probe type ultrasonicator for 5 min to form black dispersions of the nanoparticles. Two drops of each of the dispersions were dispensed on a clean Silicon (100) wafer and then air-dried. These wafers were used to obtain SEM data. For collection of STEM data, the suspensions were dried on a TEM grid. To measure the surface area of the samples, a Micromeritics ASAP 2020 was used to collect a partial adsorption isotherm at liquid nitrogen temperature (−196 °C), with krypton as the adsorption gas over the pressure range (P/P_0) of 0.06−0.5. Prior to measurements, the sample was degassed under vacuum at room temperature for 48 h. The specific surface area was determined according to the Brunauer−Emmett−Teller (BET) method.

Electrocatalytic Activity. The electrocatalytic activity of the PtBi and PtPb nanoparticles was tested using formic acid and methanol as fuels. Prior to each experiment, a suspension of the nanoparticle catalyst (referred to as catalyst ink throughout the text) was prepared as follows: to 4 mg of the dried PtBi or PtPb nanoparticle sample were added 3.98 mL of distilled water and 1 mL of isopropyl alcohol (Aldrich). Additionally, 20 μL of a 5% w/w Nafion solution in alcohols (Aldrich, EW: 1100) and water was added to this mixture. The resulting mixture was sonicated in a bath type ultrasonicator for 1 h. For the study of the oxidation of formic acid, the PtPb catalyst ink was ultrasonicated for 6 h. To study sonication time dependence on the electrochemical activity of PtPb nanoparticles, we ultrasonicated the catalyst ink for 30 min and 1.5, 2, 3,

(33) Leonard, B.; Bhuvanesh, N. S. P.; Schaak, R. E. *J. Am. Chem. Soc.* **2005**, *127*, 7326.

4, 5, 6, 7, 8, 9, and 10 h. After each time period, a drop of the sonicated catalyst ink was coated onto a clean Si (100) wafer, and SEM images of the catalyst ink were obtained. Suspensions of Pt nanoparticles (Alfa Aesar, HiSPEC TM 1000, ADS = 2−3 nm, surface area = 27 m^2/g), PtBi nanoparticles, and 50 wt % 1:1 alloy PtRu nanoparticles on a Vulcan XC-72R (E-TEK, surface area = 107 m^2/g[34]) were prepared using the same method.

Each nanoparticle suspension described above was coated onto a 3 mm diameter glassy carbon (GC) electrode. The electrode had been previously polished with diamond paste (METADI−Buehler, ø = 1μm) and ultrasonicated in Millipore water (18 MΩ cm^{-1}, Millipore Milli-Q) for 10 min. The electrode was then rinsed with Millipore water and allowed to dry in air. 70 $\mu g\ cm^{-2}$ of the nanoparticles (6.1 μL of nanoparticle suspension) was coated onto the clean glassy carbon electrode. The electrode was then spin-dried at 600 rpm under a nitrogen gas atmosphere. Before the fuel oxidation was studied, electrochemical pretreatment of all nanoparticle-coated electrodes was done by cycling the electrodes between −0.2 and 0.2 V for 10 cycles at 10 mV s^{-1} in 0.1 M H_2SO_4 (J. T. Baker ultrapure reagent).

Formic acid oxidation on the nanoparticle-coated GC electrode was examined in a mixture of 0.5 M formic acid (Mallinckrodt, 88% analytical reagent) and 0.1 M sulfuric acid at a sweep rate of 10 mV s^{-1}. Similarly, methanol oxidation at the nanoparticle-coated GC electrode was examined in a mixture of 0.5 M methanol (Burdick and Johnson, 99.9% purity) and 0.1 M sulfuric acid at a sweep rate of 10 mV s^{-1}. All solutions were prepared with Millipore water and deaerated with prepurified nitrogen for at least 10 min before each experiment. The measurements were conducted at room temperature. All potentials are referenced to a sodium-chloride-saturated Ag/AgCl electrode without regard for the liquid junction.

Results and Discussion

Because the standard reduction potentials of pure Bi, Pb, and Pt are +0.31, −0.13,V and +1.3 V, respectively,[35] Pt is more easily and rapidly reduced than both Bi and Pb. Thus, to achieve coreduction of the metals, we needed a suitably strong reducing agent; if not, selective reduction of the metals would occur and, consequently, instead of the ordered intermetallic compound PtPb (or PtBi), only Pt and/or Pb (or Bi) nanoparticles would be formed. $NaBH_4$ is apparently such a strong reducing agent, in that it unselectively reduces all metal ions so as to form the required intermetallic phases. Figures 1 and 2 show the powder X-ray diffraction (pXRD) patterns of PtPb and PtBi nanoparticles, respectively, that were formed by the coreduction of suitable precursors in methanol solvent, using $NaBH_4$ as the reducing agent. pXRD patterns in both Figures 1 and 2 indicate the formation of pure phases of PtPb (ICDD PDF file no. 06-0374) and PtBi,[36] respectively. The domain sizes of the nanoparticle products were calculated using the Scherrer formula: size (nm) = 0.94(0.154/fwhm)cos θ, where fwhm and cos θ values are in radians; the sizes were found to be 10.6 nm for PtPb and 13 nm for PtBi.

The surface areas of PtPb and PtBi nanoparticles were measured by collecting a partial adsorption isotherm at liquid nitrogen temperature, using krypton as the adsorbing gas. The specific surface areas were determined according to the Brunauer−Emmett−Teller (BET) method in the relative pressure range (P/P_0) of 0.12−0.25 for PtPb and 0.06−0.5 for PtBi. The BET surface areas for PtPb and PtBi were found to be 2.4 and 8.6 m^2/g, respectively. The *c* values (reflecting the strength of interaction between the krypton and the surface) for PtPb and PtBi were 20.18 and 20.17, respectively, whereas the correlation coefficient of the BET fit was 0.999928 for PtPb and 0.999904 for PtBi. From these data, the particle size of the products was calculated to be 152 nm (for PtPb) and 45 nm (for PtBi). The higher value of the particle size as compared to the crystal domain size is due to the aggregation of the nanoparticles to form larger networks. Table 1 lists the domain and particle sizes of the products, as determined by the Scherrer equation and from BET surface area data as well as atomic compositions determined by EDX.

SEM images of the two products were obtained by dispersing the samples in degassed isopropyl alcohol and drying the suspensions on silicon (100) wafers. Panels a and

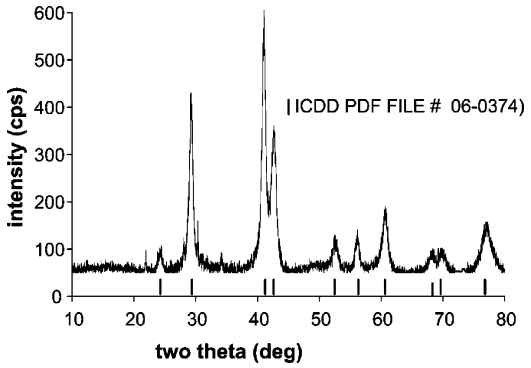

Figure 1. pXRD pattern of PtPb nanoparticles prepared by reducing H_2PtCl_6 and $Pb(MOEEAA)_2$ with $NaBH_4$ in anhydrous methanol. The markers indicate peaks for PtPb (ICDD PDF file no. 06-0374).

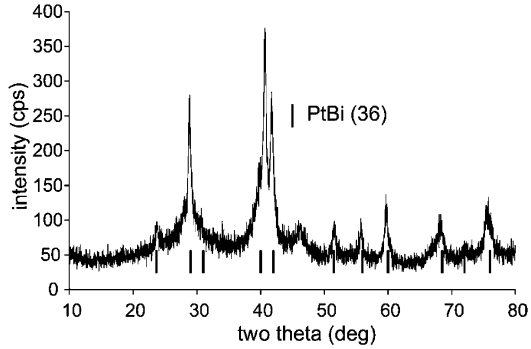

Figure 2. pXRD pattern of PtBi nanoparticles prepared by reducing H_2PtCl_6 and $Bi(MOEEAA)_3$ with $NaBH_4$ in anhydrous methanol. The markers indicate peaks for PtBi.[36]

Table 1. Domain Size (from Scherrer equation), Particle Size (from BET surface area), Surface Area, and Composition (from EDX) of PtPb and PtBi Nanoparticles

	domain size (nm)	BET surface area (m^2/g)	particle size (nm)	composition (atom %)
PtPb	10.6	2.4	152	Pt: 51 ± 1.3, Pb: 47 ± 1.2, O: 2 ± 0.3
PtBi	13	8.6	45	Pt: 45.5 ± 0.6, Bi: 50.5 ± 0.6, O: 4 ± 0.2

(34) Chai, G. S.; Yoon, S. B.; Choi, J. H.; Sung, Y. E. *J. Phys. Chem. B* **2004**, *108*, 7074.
(35) Lide, D. R. *CRC Handbook of Chemistry and Physics*, 73rd ed.; CRC Press: Boca Raton, FL, 1992; pp 8−18 and 20.
(36) Zhuravlev, N. N.; Stepanova, A. A. *Sov. Phys.−Crystallogr.* **1962**, *7*, 241.

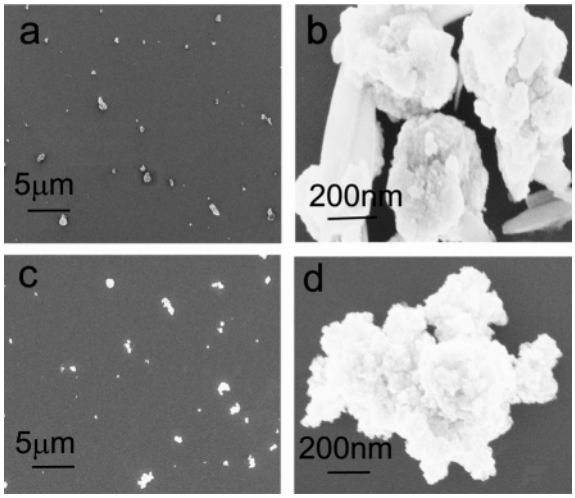

Figure 3. SEM images of (a and b) PtPb nanoparticles and (c and d) PtBi nanoparticles.

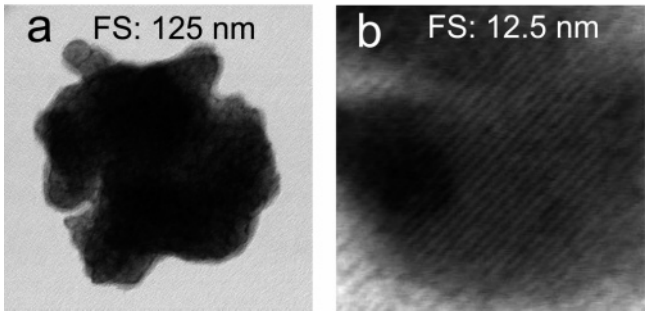

Figure 4. STEM images of PtPb nanoparticles (a) low-resolution image and (b) high-resolution image.

b of Figure 3 show low- and high-resolution SEM images for PtPb, whereas panels c and d of Figure 3 show that for PtBi. It is evident from the images that in both the cases, the nanoparticles are unaggregated on a micrometer-sized scale (see panels a and c of Figure 3). However, on a nanosized scale, the individual nanoparticles are aggregated (see panels b and d of Figure 3), forming larger networks; this is consistent with the particle size data obtained from BET measurements and X-ray diffraction measurements.

UHV−STEM analysis was performed on the products by drying the suspensions described above on a TEM grid. Panels a and b of Figure 4 show low- and high-resolution STEM images for the PtPb sample. In Figure 4b, the lattice fringes for the PtPb nanoparticles can be clearly seen. From the figure, the *d* spacing can be measured to be about 3.6 Å, which corresponds well with the (110) plane for PtPb (space group 194, $P6_3/mmc$, $a = 4.259$ Å, $c = 5.267$ Å). Panels a and b of Figure 5 show low- and high-resolution STEM images for the PtBi sample. Again, it is evident that the PtBi nanoparticles are present as aggregates.

Semiquantitative EDX spectra were taken in the STEM for both samples. The analysis was carried out for the whole region on the TEM grid that was covered by the dispersed sample, as well as for individual clusters and particles. Table 1 summarizes the elemental composition for both PtPb and PtBi. It can be seen from the EDX data (Table 1) that in both the samples, the elements are present in roughly a 1:1 ratio. The EDX data, however, also indicate the presence of

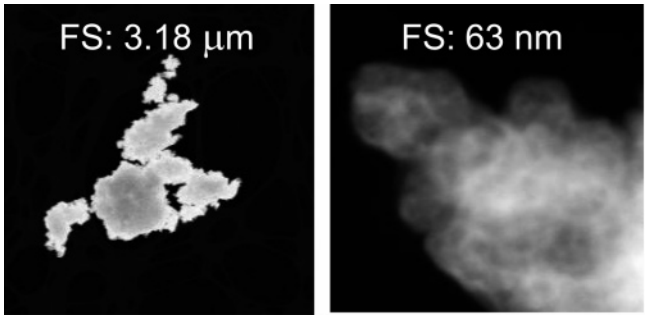

Figure 5. STEM image of PtBi nanoparticles: (a) low-resolution image and (b) high-resolution image.

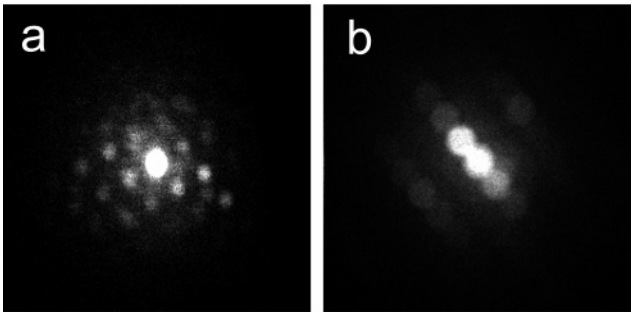

Figure 6. Convergent beam electron diffraction (CBED) pattern of (a) PtPb and (b) PtBi nanoparticles.

small amounts of oxygen, which could be due to surface oxidation of the nanoparticles as well as the copper-oxide-coated TEM grid. In fact, when the nanoparticles were first exposed to air after synthesis and drying, smoke evolution was seen near the nanoparticle surface, and the tube containing the samples became hot to the touch. This could be responsible, at least in part, for partial sintering of the large surface area of the nanoparticles in the presence of air, which would explain both the aggregated clusters and the presence of oxygen in the EDX spectrum. However, pXRD patterns of the PtPb nanoparticles taken before exposing them to air (using a special holder designed and built in our laboratory) showed only peaks corresponding to PtPb, with a domain size around 11 nm. This implies that the heat/smoke that occurred when the nanoparticles were exposed to air was caused by surface oxidation of the nanoparticles, but that the heat does not play a significant role in increasing the particle size by sintering. This in turn implies that about 10 nm single crystals of ordered intermetallic PtPb nanoparticles were formed at room temperature, which then further aggregate to form networks. The smallest PtPb and PtBi particles are single-crystal domains, as shown by the CBED pattern (Figure 6a for PtPb, and Figure 6b for PtBi).

Figure 7 shows the rotating disk electrode voltammograms for formic acid oxidation on four different nanoparticle catalyst electrodes: Pt, PtRu supported on carbon, PtPb, and PtBi (see the Experimental Section). In comparing the relative activity of these electrocatalysts, we find that two parameters are of significance: onset potential (which reflects thermodynamic aspects) for fuel oxidation and current density (which reflects kinetic aspects) at a given potential. Thermodynamically, the onset of formic acid oxidation should occur near −0.2 V (vs NaCl-saturated Ag/AgCl

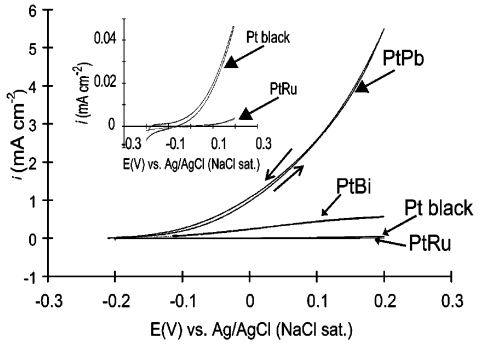

Figure 7. Rotating disk voltammograms for formic acid oxidation on 4 nm Pt black, 10 nm PtPb nanoparticles, 13 nm PtBi nanoparticles, and 1:1 PtRu alloy nanoparticles on Vulcan XC72R, as labeled. Inset shows voltammograms scaled to reveal Pt and PtRu activity (note expanded *y*-axis scale). All data measured for 0.5 M formic acid in 0.1 M sulfuric acid (electrode rotation rate = 2000 rpm, potential scan rate = 10 mV s^{-1}).

Table 2. Onset Potentials and Current Densities at Different Voltages for Pt Black, PtRu/C, PtPb, and PtBi Nanoparticles for Formic Acid Oxidation (all specified potentials are vs Ag/AgCl (NaCl sat.))

catalyst	onset potential (mV)	current density (mA cm^{-2})			
		−100 mV	0 mV	+100 mV	+200 mV
Pt black	+000	0	0.003	0.018	0.05
PtRu	+200	0	0	0.0007	0.003
PtBi	−200	0.065	0.22	0.44	0.56
PtPb	−200	0.18	0.87	2.6	5.5

electrode). Good catalysts are those with low overpotentials for oxidation, so that high oxidation currents occur at potentials only slightly more positive than −0.2 V. Therefore, the higher the current density at a given potential, the better the catalyst.

For formic acid oxidation, the Pt, carbon-supported PtRu, PtBi, and PtPb nanoparticle electrodes exhibited onset potentials of 0, +200, −200, and −200 mV, respectively (see Table 2). These values suggest that nanoparticles of both PtBi and PtPb have superior electrocatalytic activity when compared to both Pt and PtRu. Additionally, the onset potentials of PtPb and PtBi nanoparticles are in accordance with the values obtained for bulk PtPb and bulk PtBi samples,[18,19] indicating that, thermodynamically, the catalytic properties of these materials are retained at the 10 nm and above scale.

Table 2 also lists the current densities (in terms of mA cm^{-2}) of the four catalysts at four specific potentials. This value is a direct measure of electrocatalytic efficiency. In this study, all four of the electrocatalyst materials examined had different particle sizes and, consequently, different surface areas and specific surface areas. Furthermore, electrochemical protocols for the measurement of the specific surface area for these novel intermetallic nanoparticles have not been established. This is in contrast to Pt, for which methods are well-established (e.g., coulombic integration of hydrogen adsorption). To make the most-meaningful comparison of the raw current data collected, we normalized currents to the measured BET surface area of the respective catalysts (results are listed earlier in this section and in the Experimental Section). The resulting surface area normalized current densities appear in plots and in the tables as mA cm^{-2} (where cm^2 is the BET surface area for the catalyst charge on the GC electrode). From the values presented in Table 2

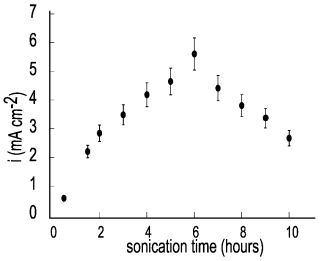

Figure 8. Plot of current density (at 0.2 V) vs. sonication time for a PtPb nanoparticle ink for formic acid oxidation activity.

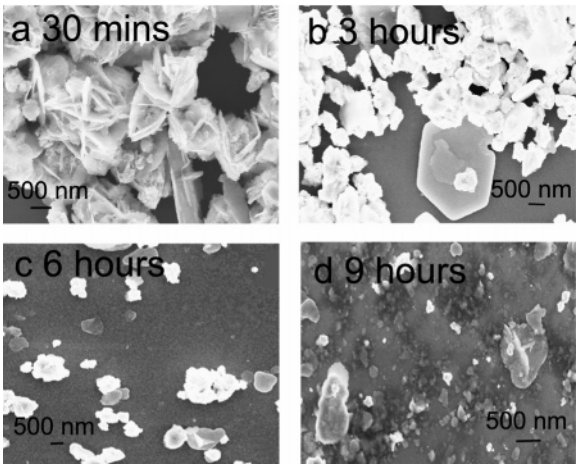

Figure 9. SEM images of PtPb nanoparticle ink taken after different sonication times of (a) 30 min, (b) 3 h, (c) 6 h, and (d) 9 h.

for formic acid oxidation, it is evident that both PtPb and PtBi have activities that are far superior to those of carbon-supported PtRu and Pt. PtPb, in particular, exhibits a current density that is 2 orders of magnitude higher than the commercially available electrocatalysts. In the case of PtBi, the results are consistent with those we reported earlier for PtBi nanoparticles prepared by the polyol process.[37] In the present case, the activity for PtBi is slightly elevated; however, we believe this is due to enhanced surface area.

The electrocatalytic activity for the oxidation of formic acid by PtPb nanoparticles was also studied as a function of sonication time of the catalyst ink. The intent was to see if the sonication process resulted in morphological changes that affected electrocatalytic activity. Figure 8 shows the current density at 0.2 V as a function of the sonication time. It can be seen from the figure that the current density first increases with sonication time, peaks at around 6 h, and then decreases with further sonication. To gain a clearer understanding of this phenomenon, aliquots of the inks were withdrawn after each sonication period (11 samples), and SEM images were obtained after coating them on Silicon (100) wafers and drying them (see the Experimental Section). Figure 9 shows SEM images that were obtained for the same ink after four different sonication times. It can be seen from the figures that the morphology of the particles in the ink changes with sonication time. For short sonication times (30 min, Figure 9a), the nanoparticles in the ink are highly aggregated with platelike and needlelike morphologies. The aggregates are also quite large, reaching micrometer dimensions. Increased

(37) Roychowdhury, C.; Matsumoto, F.; Mutolo, P. F.; Abruña, H. D.; DiSalvo, F. J. *Chem. Mater.* **2005**, *17*, 5871.

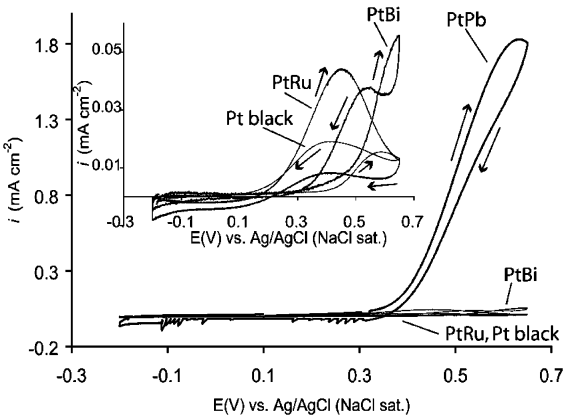

Figure 10. Rotating disk voltammogram for methanol oxidation on 4 nm Pt black, 10 nm PtPb nanoparticles, and 1:1 PtRu alloy nanoparticles on Vulcan XC72R, as labeled. Inset shows voltammograms on an expanded current scale to reveal Pt, PtRu, and PtBi activity (note expanded *y*-axis scale). All data measured for 0.5 M methanol in 0.1 M sulfuric acid (electrode rotation rate = 2000 rpm, potential scan rate = 10 mV s^{-1}.

sonication (e.g., 3 h, Figure 9b, and 6 h, Figure 9c) causes some of the particles to break up into smaller aggregates. The morphology also begins to change (Figure 9b). Further sonication causes most of the aggregates to break apart, resulting in much smaller particles on the order of half a micrometer or less. This trend of gradually breaking down the agglomerated masses into discrete particles results in an expected increase in catalyst surface area. Consequently, the measured current density for formic acid oxidation increases. This trend reaches a maximum of active surface area (as measured by current density) at 6 h. Beyond this point, further sonication causes the activity to drop (see Figure 9). The SEM image after 9 h of sonication (Figure 9d) shows degradation and decomposition of the nanoparticles in the ink. The particles no longer appear crystalline (associated with bright white color as seen in the previous pictures), but gray and amorphous. The particle size also increases again, perhaps due to sintering caused by the generation of high levels of local heat from prolonged sonication. Furthermore, the Pb from PtPb could be leaching out of the sample by reaction with oxygen to form oxides on the surface (as the solution was purged only periodically during sonication), which would also be responsible for a decrease in activity. Thus, it appears that under the current conditions, a 6 h sonication time is the optimal value for obtaining high current density for the as-prepared PtPb nanoparticles.

Figure 10 presents the rotating disk electrode voltammograms obtained for methanol oxidation on nanoparticles of Pt, carbon-supported PtRu, PtPb, and PtBi. In this case, onset potentials of 400, 180, 300 , and 300 mV, respectively, were obtained. Table 3 summarizes the onset potentials and surface area normalized current densities at several potentials for the four samples. An initial analysis of these results reveals that PtRu has the lowest onset potential of the four electrocatalysts. However, the benefit of the much enhanced current density of PtPb far outweighs its somewhat elevated (ΔE = +120mV) onset potential relative to PtRu. Indeed, PtPb exhibits an increase of 1−2 orders of magnitude in current density over both commercial PtRu and Pt black. The results also show that in terms of current density, PtBi is not a very

Table 3. Onset Potentials and Current Densities at Different Voltages for Pt Black, PtRu, PtPb, and PtBi Nanoparticles for Methanol Oxidation (all specified potentials are vs Ag/AgCl (NaCl sat.))

catalyst	onset potential (mV)	current density (mA cm^{-2}) +400 mV	+450 mV	+500 mV	+600 mV
Pt black	+400	0	0.004	0.01	0.016
PtRu	+180	0.04	0.044	0.04	0.018
PtBi	+300	0.005	0.008	0.013	0.05
PtPb	+300	0.18	0.5	0.94	1.75

active catalyst for methanol oxidation. This is consistent with earlier results on bulk PtBi samples.[18]

It is also important to note the shape of the voltammograms. PtRu and PtBi exhibit a great deal of hysteresis (see the inset of Figure 10), whereas PtPb exhibits less, especially at lower potentials. Also, PtBi exhibits a great deal of tolerance to CO, whereas PtPb exhibits slightly less tolerance to CO as compared to PtBi.[38]

From the above discussion, it is evident that PtBi and PtPb nanoparticles are far superior in performance to both Pt and PtRu for formic acid oxidation in terms of onset potential and current density. Both PtPb and PtBi exhibit significant negative shifts in onset potential for the oxidation of formic acid compared to Pt (ΔE = −200 mV) and PtRu (ΔE= −400 mV). Both catalysts, and especially PtPb, exhibit dramatically higher current densities compared to those of Pt and PtRu (see Table 2). For methanol oxidation, whereas PtRu exhibits a lower onset potential compared to PtBi and PtPb (ΔE = 120 mV), the current densities of the latter samples are far superior to both Pt and PtRu.

In electrochemical environments, metals typically dissolve in aqueous media near their standard reduction potentials (E^0), unless a passivating layer forms on the metal surface. The exact potential of dissolution depends on the metal-ion concentration in the solution, shifting to more-negative values (following the Nernst equation) as the ion concentration is lowered.[39] Metals that have negative E^0 values can react with water to release H_2 at low pH, whereas those with E^0 below 1.2 V usually form oxides in air, at least on their surfaces. Kinetics determine the rate of oxide formation and the oxide film thickness. In many cases, a thin layer of oxide forms on the surface, passivating the metal surface to further oxidation. In the case of Bi and Pb, the E^0 values are 0.31 and −0.13 V, respectively. This implies that Bi ions would leach out into solution near 0.31 V and that Pb ions would do so at much lower potentials. However, these metals are stabilized against dissolution by forming intermetallic compounds. For the formation of ordered intermetallic platinum compounds (MPt), the free energy of formation ΔG^0_f(MPt) < 0. If E^0(M) < E^0(Pt), then M will dissolve at lower potentials than Pt, but E^0(M) is now shifted to more-positive potentials by $\Delta E = -\Delta G^0_f/zF$.[40] In alloys such as Pt−Ru, $\Delta G^0_f \approx 0$, and thus there is virtually no stabilization of Ru against dissolution by alloy formation. In ordered interme-

(38) de-los-Santos-Álvarez, N.; Alden, L. R.; DiSalvo, F. J.; Abruña, H. D. CO tolerance of ordered intermetallic phases; to be submitted.
(39) Bard, A. J.; Faulkner, L. R. *Electrochemical Methods, Fundamentals and Applications*, 2nd ed.; John Wiley & Sons: New York, 2001.
(40) Gaskell, D. R. *Introduction to Metallurgical Thermodynamics*, 2nd ed.; Hemisphere Publishing Corporation: Newport, Australia, 1981.

tallic compounds, the ΔG^0_f value can be quite large, and stabilization up to 1.0 V is possible. For example, the $<\Delta G^0_f$ of PtBi is approximately −63 kJ/mol (calcd[41]), giving rise to a stabilization on the order of 220 mV. Hence, the E^0 for Bi dissolution from PtBi now becomes +0.53 V. Similarly, the ΔG^0_f of PtPb is approximately −51 kJ/mol (calcd[41]); thus $\Delta E = +260$ mV so that the E^0 for PtPb is now +0.13 V, which implies that PtPb is stable at low pH and will not react to release H_2. Thus, at low potentials, which are the ideal operating conditions for PEM fuel cells, the use of ordered intermetallic phases such as PtPb and PtBi will mitigate the leaching out of metal ions in solutions, which may cause degradation of the catalyst and/or deactivation of the membrane by exchange, resulting in a loss of fuel-cell efficiency.

Finally, it is also important to note that the synthesis conditions have not been optimized for preparing nanoparticles of intermetallic phases. This is to be compared and contrasted with Pt black and especially carbon-supported PtRu (from E-TEK), which have been extensively explored and optimized for fuel-cell applications. Yet, even under these nonoptimized conditions, PtBi and PtPb still exhibit superior activity for formic acid oxidation when compared with commercially available fuel-cell catalysts. Thus, at this time, the dramatic activity enhancements exhibited can still be considered as being lower limits.

Conclusions

We have demonstrated a new low-temperature solvent-phase approach to the synthesis of crystalline nanoparticles of two ordered intermetallic phases, PtBi and PtPb. In this approach, anhydrous methanol was used as the solvent and $NaBH_4$ as the reducing agent. Because of the limited solubility of most Bi and Pb precursors in anhydrous methanol, metal salts of a solubilizing acid, (2-[2-{2-methoxy}ethoxy]ethoxy)acetic acid (MOEEAA), were used as starting precursors. Powder X-ray diffraction (pXRD) studies confirmed the presence of the ordered intermetallic phases of PtPb and PtBi, with average domain sizes of 10 and 13 nm, respectively. Electron microscopy was used to study the morphology of the nanopowders; it showed that the nanoparticles were present as aggregated networks. Electron diffraction studies showed the smallest nanoparticles to be present as single-crystal domains. The BET surface areas of PtPb and PtBi nanoparticles were found to be 2.4 and 8.6 m^2/g, respectively, which was consistent with the size of the aggregated networks. The as-prepared PtPb and PtBi nanoparticles exhibited enhanced electrochemical activity when compared to that of commercially available Pt and PtRu nanoparticles in terms of current density for methanol oxidation and current density and onset potential for formic acid oxidation. The electrocatalytic activity toward formic acid oxidation of the PtPb nanoparticles was studied as a function of sonication time of the catalyst ink, and with nanoparticle morphology changes followed by scanning electron microscopy. The results showed that the activity of the catalyst initially increased with sonication time, peaked at 6 h, and then decreased with increasing time of sonication. This increase is likely due, at least in part, to an increase in surface area with sonication time, whereas the decrease in activity occurred as the crystallinity and surface integrity was lost after extensive sonication.

Acknowledgment. This work was supported by DOE Grant DE-FG02-03ER46072. The STEM, microprobe, and SEM data were obtained in the shared experimental facilities managed by the Cornell Center for Materials Research, a MRSEC center supported under NSF Grant DMR-05779992. C.R.C. would like to thank Malcolm Thomas at the Cornell Center for Materials Research for help with the STEM data collection. C.R.C. also thanks Scott Warren at the Materials Science and Engineering Department at Cornell University for helping with the BET surface area measurements and with the synthesis of Bi and Pb MOEEAA compounds. M.J.B. thanks the Cornell Center for Materials Research REU program for support in the summer of 2005.

CM060480E

(41) Miedema, A. R.; Dechâtel, de Boer, F. R. *Physica B* **1980**, *100*, 1.